Supporting Information

Hypercrosslinked polymer-mediated fabrication of binary metal phosphides decorated spherical carbon as efficient and durable bifunctional electrocatalyst for rechargeable Zn-air batteries

Haowen Chen, Yijiang Liu, * Bei Liu, Mei Yang, Huaming Li, and Hongbiao Chen, *

College of Chemistry, Key Lab of Environment-Friendly Chemistry and Application in Ministry of Education, Key Laboratory of Polymeric Materials and Application Technology of Hunan Province, Xiangtan University, Xiangtan 411105, Hunan Province, P. R. China.

E-mail: liuyijiang84@xtu.edu.cn (Y Liu), chenhongbiao@xtu.edu.cn (H. Chen),

Experimental Section

1. Materials

Iron(III) nitrate, and nickel(II) nitrate were purchased from Shanghai Aladdin Bio-Chem Technology Co., Ltd. Phytic acid and ethanol were purchased from Shanghai Macklin Biochemical Co., Ltd. All the chemicals were analytical agent grade and used as received.

2. Optimization of synthetic condition for FeCoP/NPC electrocatalysts

2.1. Optimization of pyrolysis temperature

The synthesis process is similar to that of FeCoP/NPC electrocatalyst, except the carbonization temperature (800 °C, 900 °C, 1000 °C) are different. The synthesized FeCoP/NPC electrocatalysts are named FeCoP/NPC-800, FeCoP/NPC-900 and FeCoP/NPC-1000 respectively.

2.2. Optimization of pyrolysis time

The synthesis procedures were similar to that of FeCoP/NPC electrocatalyst except for different pyrolysis time at 900 °C. That is for 1, 2 and 3 h under N_2 blowing conditions. The resultant FeCoP/NPC electrocatalysts were named as FeCoP/NPC-1h, FeCoP/NPC-2h, and FeCoP/NPC-3h, respectively.

2.3. Optimization of FeCo/HCTCz mass ratios

The synthesis procedures were similar to that of FeCoP/NPC electrocatalyst except that the mass ratio of the polymer HCTCz to the total mass of Fe/Co was set to 1:10, 1:12 and 1:14, respectively. The resultant FeCoP/NPC electrocatalysts were denoted as FeCoP/NPC-1:10, FeCoP/NPC-1:12 and FeCoP/NPC-1:14, respectively.

2.4. Optimization of Fe/Co molar ratio

The synthesis procedures were similar to that of FeCoP/NPC electrocatalyst except for different Fe/Co molar ratio, the Fe/Co molar ratio was varied from 2:1, 1:1,

to 1:2, while the total molar amount of $Fe(NO_3)_3$ and $Co(NO_3)_2$ was remain unchanged. The resultant FeCoP/NPC electrocatalysts were named as FeCoP/NPC-2:1, FeCoP/NPC-1:1, and FeCoP/NPC-1:2, respectively.

2.5. Optimization of FeCo/PA mass ratio

The synthesis procedures were similar to that of FeCoP/NPC electrocatalyst except for varied amount of PA. The mass ratio of the Fe/Co to PA was regulated to be 1:3, 1:2.25 and 1:1.5, respectively. The resultant FeCoP/NPC electrocatalysts were denoted as FeCoP/NPC-1:3, FeCoP/NPC-1:2.25 and FeCoP/NPC-1:1.5, respectively.

3. Characterization

The textural properties were characterized by N_2 adsorption/desorption measurements at 77.3 K using Micromeritics TriStar II 3020 surface area and porosimeter analyzer. The specific surface area was calculated by using Brunauer-Emmett-Teller (BET) method. The pore size distribution (PSD) was calculated from the adsorption branches of the isotherms by using the DFT model. The powder X-ray diffraction patterns (PXRD) were collected on a Rigaku/Max-2500PC X-ray diffractometer with Cu Kα radiation, and the operation voltage and current were maintained at 40 kV and 25 mA, respectively. The X-ray photoelectron spectroscopy (XPS) was performed on a K-Alpha 1063 photoelectron spectrometer (Thermo Fisher Scientific, England) with Al-Kα X-ray radiation as the X-ray source for excitation. Scanning electron microscopy (SEM) images were recorded using S-4800 (JEOL)

operated at an acceleration voltage of 10 kV. The transmission electron microscopy (TEM) images were recorded on a JEOL-2010 transmission electron microscope (Thermo Scientific Talos F200i) operating at 200 kV.

4. Electrochemical measurements

The electrochemical experiments were conducted on a CHI760D electrochemical workstation (Chenhua Instruments Co., Shanghai) in a three-electrode system at 25 °C. A rotating disk electrode (RDE) or a rotating ring-disk electrode (RRDE) was used as the working electrode, an Ag/AgCl electrode (3 M KCl) was used as the reference electrode, and a graphite rod was used as the counter electrode in alkaline electrolyte. The fabrication of working electrode was carried out as follows: Taking FeCoP/NPC for an example, 4.0 mg catalyst was firstly dispersed in 970 μL ethanol, then 30 μL Nafion solution (5.0 wt%) was added, followed by sonication for 0.5 h to form a relatively homogeneous suspension. 12.0 μL of the catalyst inks was transferred onto the glassy carbon disk electrode; the effective mass loading on glassy carbon disk electrode was about 0.7 mg cm^{-2}. The same method was used to prepare Pt/C, but the effective mass loading on glassy carbon disk electrode is about 0.6 mg cm^{-2}. ORR activity was evaluated by linear sweep voltammetry (LSV) techniques on rotating disk electrode (RDE) in O_2-saturated 0.1 M KOH solution by flowing O_2 with varying rotating speed from 400 to 2400 rpm at a rate of 10 mV s^{-1}. All measured potentials in this study were converted to reversible hydrogen electrode (RHE) according to the following equations:

$$E_{(RHE)} = E_{Ag/AgCl} + 0.210 + 0.059 \times pH$$

The parameter of electron transfer number (n) per oxygen molecule involved in the typical ORR process was calculated from the slopes of Koutecky-Levich (K-L) equation:

$$1/J = 1/J_L + 1/J_K = 1/(B\omega^{1/2}) + 1/J_K$$

$$B = 0.2nFC_0 (D_0)^{2/3} \nu^{-1/6}$$

where J, J_L, J_k are the measured current density, the diffusion current density, and the kinetic current density, respectively. ω is the electrode rotating speed in rpm, F is the Faraday constant (96485 C mol^{-1}), D_0 is the diffusion coefficient of oxygen in 0.1 M KOH (1.9×10^{-5} cm^2 s^{-1}), ν is the kinetic viscosity (0.01 cm^2 s^{-1}), and C_0 is the bulk concentration of oxygen (1.2×10^{-6} mol cm^{-3}). The constant 0.2 is adopted when the rotation speed is expressed in rpm.

The RRDE measurements were also conducted to determine peroxide species formed and the electron transfer number (n). The ring-disk electrode was scanned at a rate of 10 mV s^{-1} and the ring electrode potential in the RRDE system was set to 1.4 V versus RHE. The yield of peroxide species (%HO_2^- in alkaline media) was calculated by the followed equations:

$$\%HO_2^- = 200 \times \frac{i_r / N}{i_r / N + i_d}$$

$$n = 4 \times \frac{i_d}{i_r / N + i_d}$$

where i_d and i_r are the disk and ring currents, respectively. N is current collection efficiency of Pt ring, which was determined to be 0.37.

The OER electrochemical measurements were also conducted in a CHI 760D workstation connected with a three-electrode system with Pt sheet and Ag/AgCl electrodes and counter and reference electrodes, respectively. However, the working electrode for OER was prepared by drop-casting the ink (prepared in a similar method to test for ORR) onto carbon paper with a surface area of 0.25 cm^{-2} and the loading of catalyst was maintained at 0.7 mg cm^{-2}. The OER performance test was obtained by polarization curves using linear scanning voltammetry (LSV) at 10 mV s^{-1} in 0.1 M KOH under saturated O_2 to provide the O_2/H_2O equilibrium at 1.23 V versus RHE (all data were reported with *iR* compensation. The OER potential was obtained by an *iR* compensation approach using the $E - iR \times 100\%$ relationship, where *i* is the current and *R* is the uncompensated electrolyte ohmic resistance). The EIS was recorded at 1.6 V in the frequencies ranged from 100 000 to 0.1 Hz with an amplitude of 5 mV and the polarization curves were plotted as potential versus $\log|j$, mA $cm^{-2}|$ to get the Tafel plots. Accordingly, the Tafel slope (b) can be obtained by fitting the linear portion of Tafel plots based on the equation of $\eta = b \log (j) + a$.

5. Zn-air batteries assembly

A home-made liquid Zn-air battery was assembled to access the battery performance. The catalyst inks were prepared as above mentioned in electrochemical measurements, which were uniformly drop-cast onto gas diffusion layer (GDL) carbon paper with catalyst loading of 1.50 mg cm^{-2}. To compare the battery performance, the rechargeable battery was also made from a mixed Pt/C (20 wt %, JM) and IrO_2 (99.9%)

(mass ratio = 1/1, Pt/C + IrO_2 loadings: 1.0 mg cm^{-2}). The reaction area of cathode is 1 cm^2. Polished zinc foil was chosen as anode in 6 M KOH + 0.2 M $Zn(OAc)_2$ electrolyte.

The solid-state Zn-air battery was fabricated by a polished zinc foil as anode, the air electrode was made by dropping a certain volume of catalyst ink onto a cleaned carbon cloth substrate with a catalyst loading of 1.5 mg cm^{-2}, gel polymer as solid electrolyte and carbon cloth as charge collector. The solid electrolyte was prepared as follow [1]: First, 9.0 g acryl amide (AM) and 3 mL GO dispersions (with concentrations at 10 mg/mL) were dispersed in 100 ml deionized water, after sonication for 20 min, the obtained solution was kept at 85 °C for 3 h under vigorous stirring. Subsequently, 10 mL acrylic acid (AA) was added and the pH of the mixture was adjusted to about 7 with NaOH solution. 0.1 g N, N'-methylenebis(acrylamide) (BIS) and 0.1 mL N, N, N', N'-Tetramethylethylenediamine (TEMED) were added for cross-linker and accelerant, respectively. Afterwards, 0.02 g initiator (ammonium persulfate) was added and stirred for 10 s. The as-obtained solution was dumped in a glassy mold. After sequent heating, removing of water and soaking in 6M KOH/0.2M $Zn(CH_2COO)_2$ alkali solution (24 h), PAM-co-PAA alkaline hydrogel electrolyte was obtained.

Figures and Tables

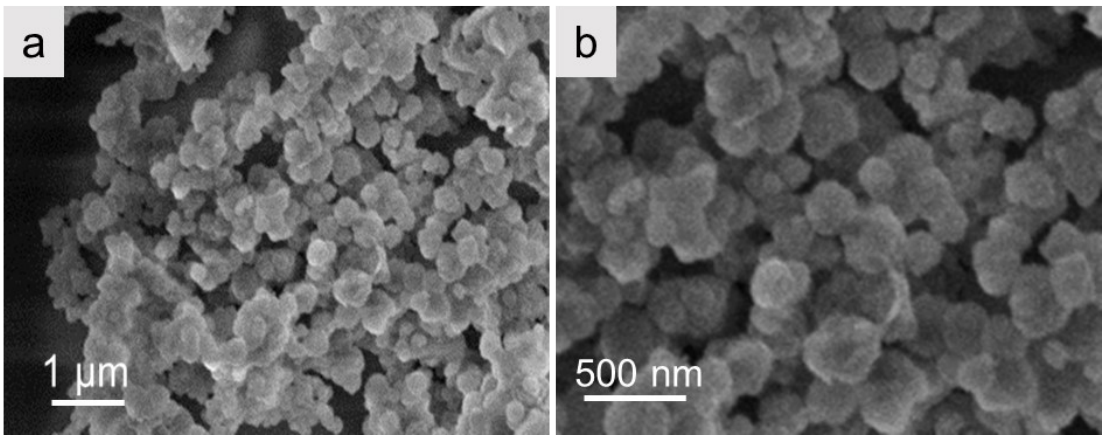

Figure S1. (a, b) SEM images of hypercrosslinked polymer HCTCz.

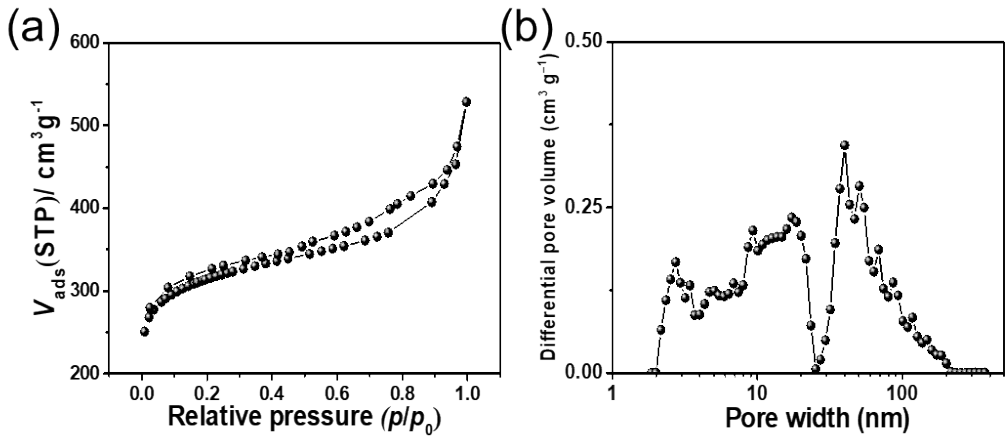

Figure S2. (a) N_2 adsorption/desorption isotherms at 77 K and (b) Pore size distribution of HCTCz.

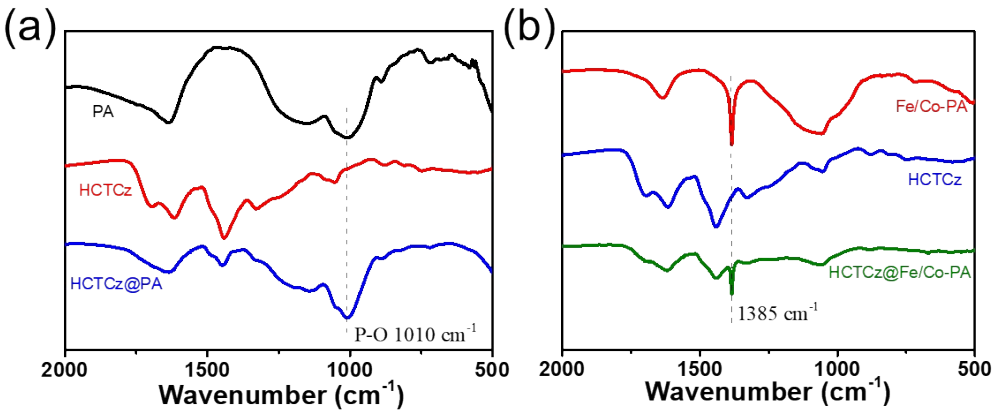

Figure S3. FT-IR spectra of (a) PA, HCTCz, HCTCz@PA and (b) Fe/Co-PA and HCTCz@Fe/Co-PA.

As shown in Figure S3, the characteristic band of P-O (1010 cm^{-1}) appeared in HCTCz@PA after the absorption of PA onto (into) HCTCz. The feature peak located at 1385 cm^{-1} indicated the complexation interaction between PA and Fe/Co, i.e., forming the HCTCz@Fe/Co-PA.

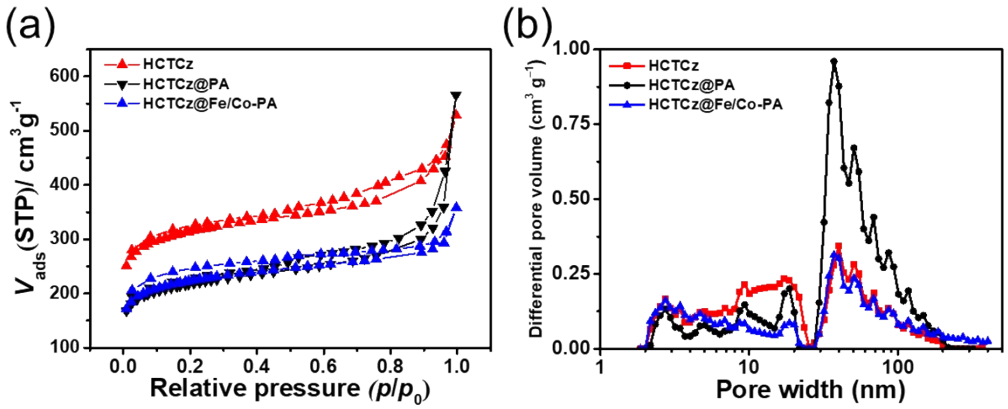

Figure S4. (a) N_2 adsorption/desorption isotherms at 77 K and (b) pore size distribution of HCTCz, HCTCz@PA and HCTCz@Fe/Co-PA.

As shown in Figure S4, the BET surface area of HCTCz, HCTCz@PA and HCTCz@Fe/Co-PA were calculated to be 989 m^2 g^{-1}, 691 m^2 g^{-1} and 715 m^2 g^{-1}, respectively. Compared with HCTCz, the decrease of the BET surface area for HCTCz@PA and HCTCz@Fe/Co-PA is mainly due to the adsorption of PA and Fe/Co-PA on the surface and (or) pores of HCTCz.

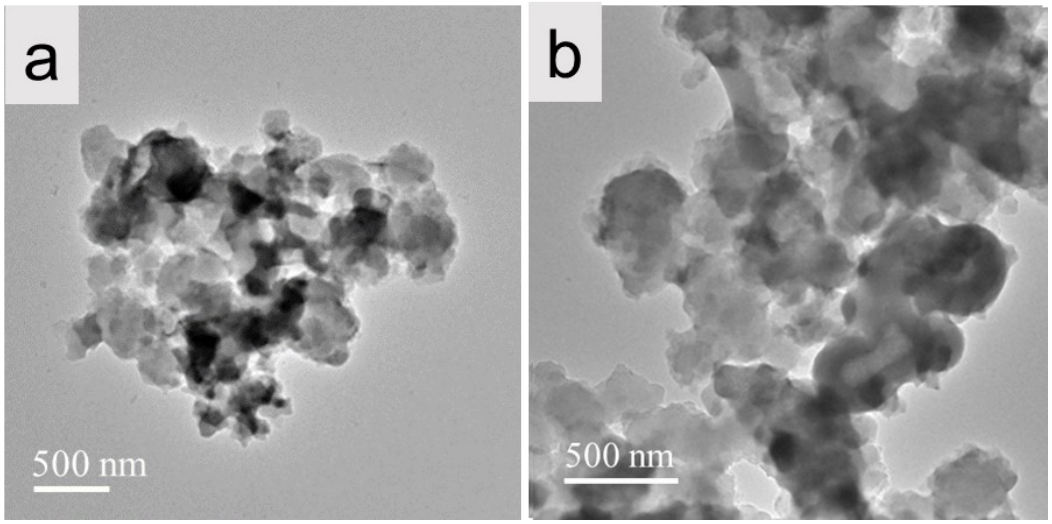

Figure S5. (a, b) TEM of HCTCz@Fe/Co-PA.

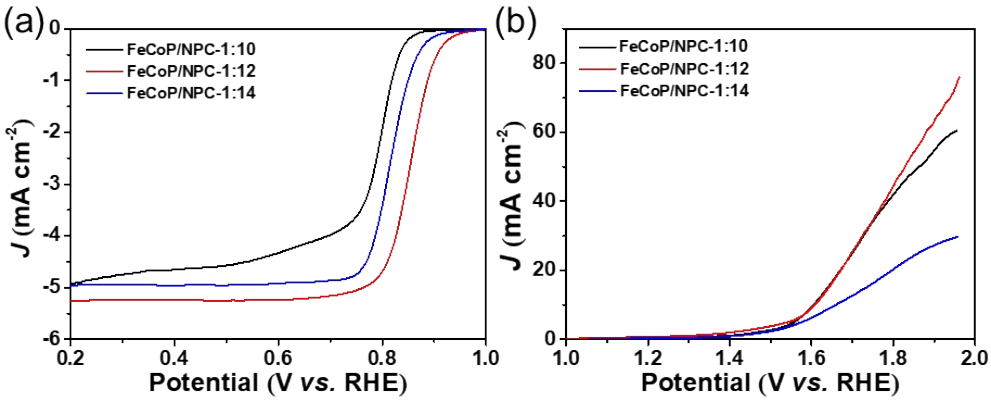

Figure S6. (a) ORR and (b) OER performance of FeCoP/NPC-1:10, FeCoP/NPC-1:12, and FeCoP/NPC-1:14 electrocatalysts. (1:10, 1:12, 1:14 denoted the different mass

ratio of FeCo to HCTCz)

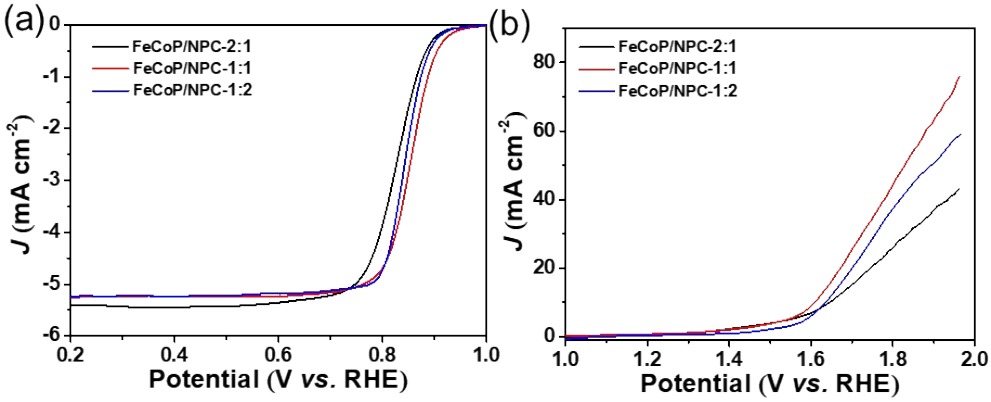

Figure S7. (a) ORR and (b) OER performance of FeCoP/NPC-1:3, FeCoP/NPC-1:2.25, and FeCoP/NPC-1:1.5 electrocatalysts. (1:3, 1:2.25, 1:1.5 represented the different mass ratio of FeCo and PA)

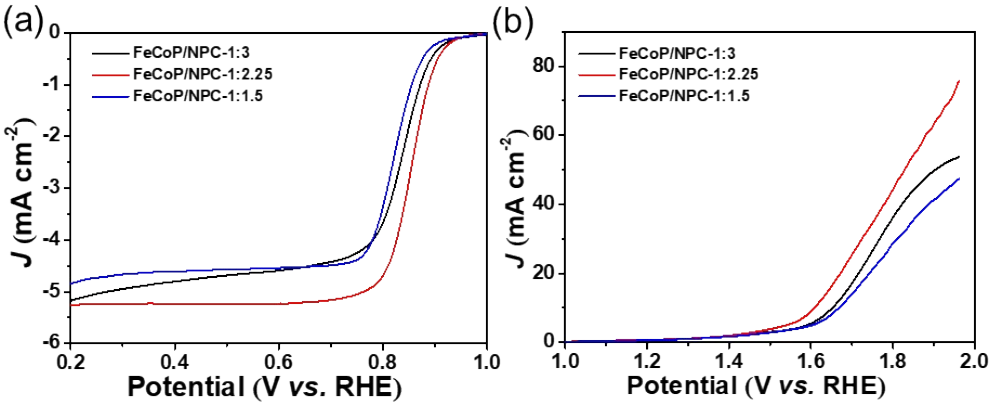

Figure S8. (a) ORR and (b) OER performance of FeCoP/NPC-2:1, FeCoP/NPC-1:1, and FeCoP/NPC-1:2 electrocatalysts. (2:1, 1:1, 1:2 denoted the different Fe/Co molar ratios)

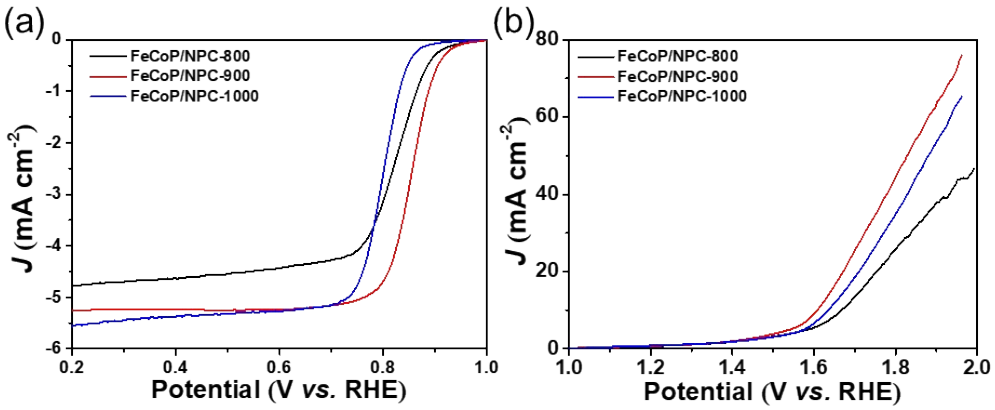

Figure S9. (a) ORR and (b) OER performance of FeCoP/NPC-800, FeCoP/NPC-900, and FeCoP/NPC-1000 electrocatalysts. (800/900/1000 denoted the different pyrolysis temperature)

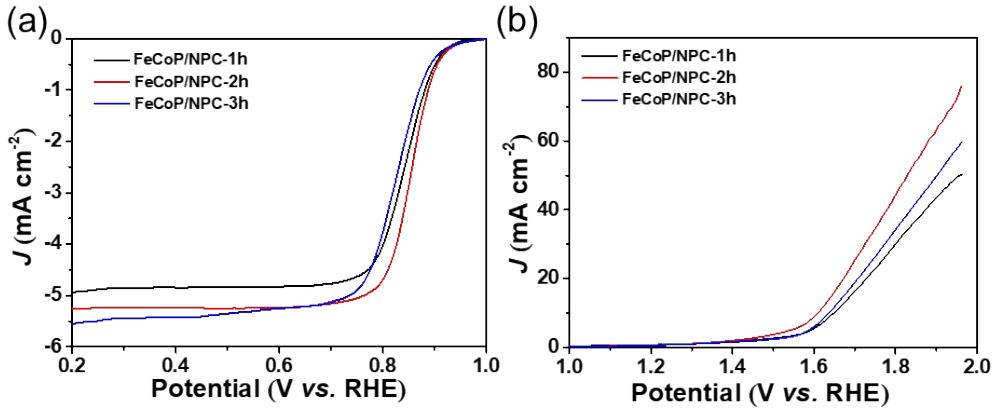

Figure S10. (a) ORR and (b) OER performance of FeCoP/NPC-1h, FeCoP/NPC-2h, and FeCoP/NPC-3h electrocatalysts. (1h/2h/3h denoted the different pyrolysis time)

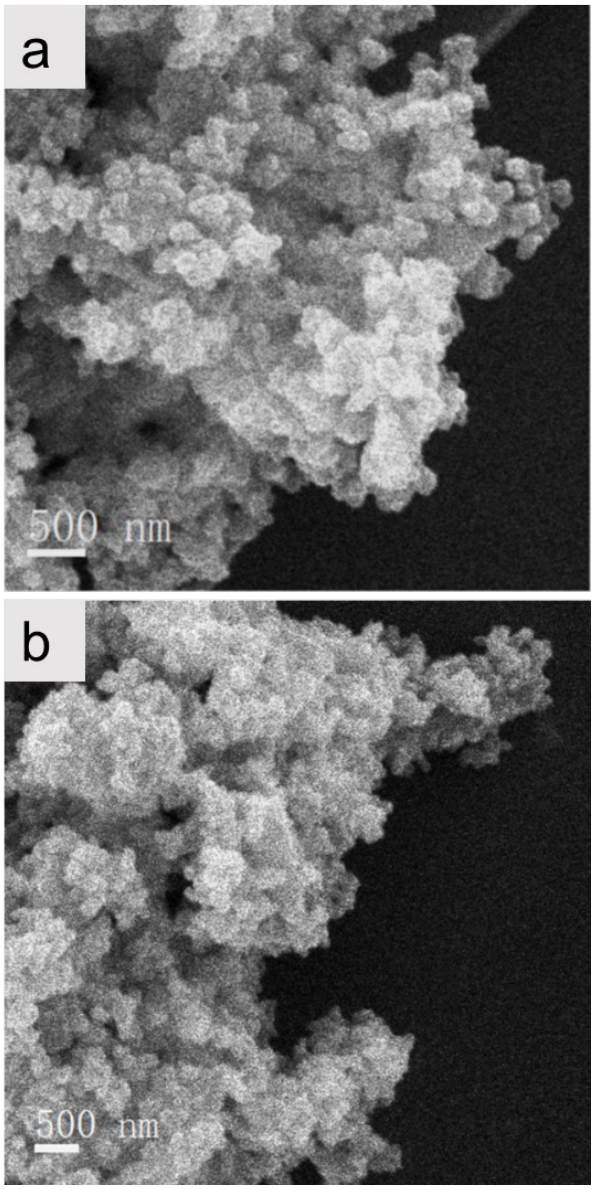

Figure S11. SEM images of (a) NC and (b) FeCo/NC.

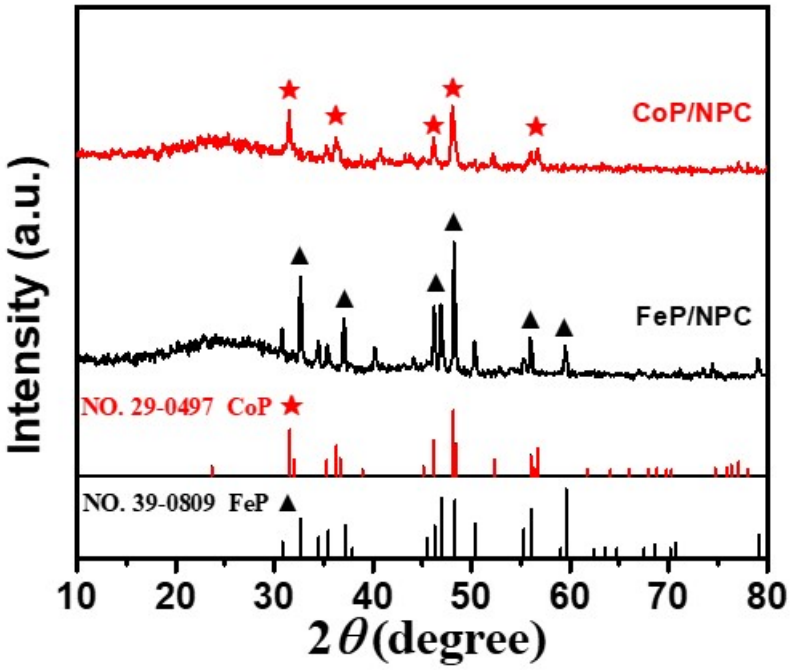

Figure S12. XRD patterns of FeP/NPC and CoP/NPC composites.

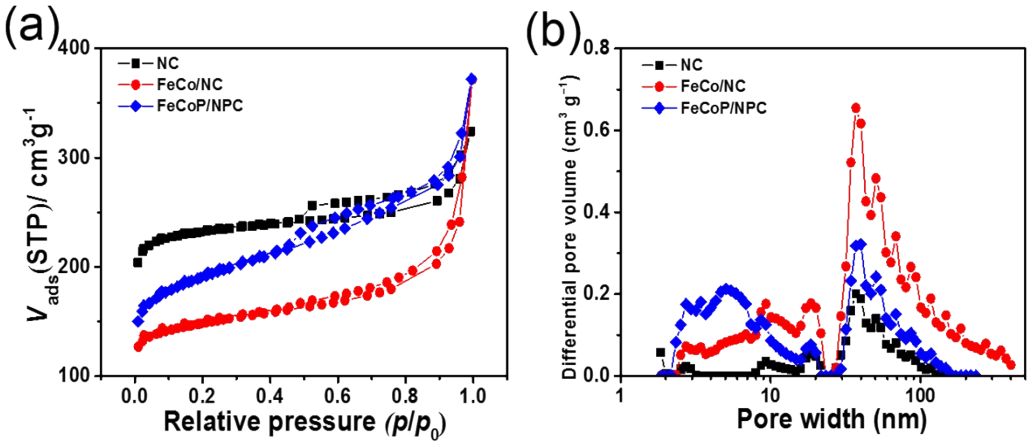

Figure S13. (a) N_2 adsorption/desorption isotherms at 77 K and (b) Pore size distribution of NC, FeCo/NC and FeCoP/NPC electrocatalysts.

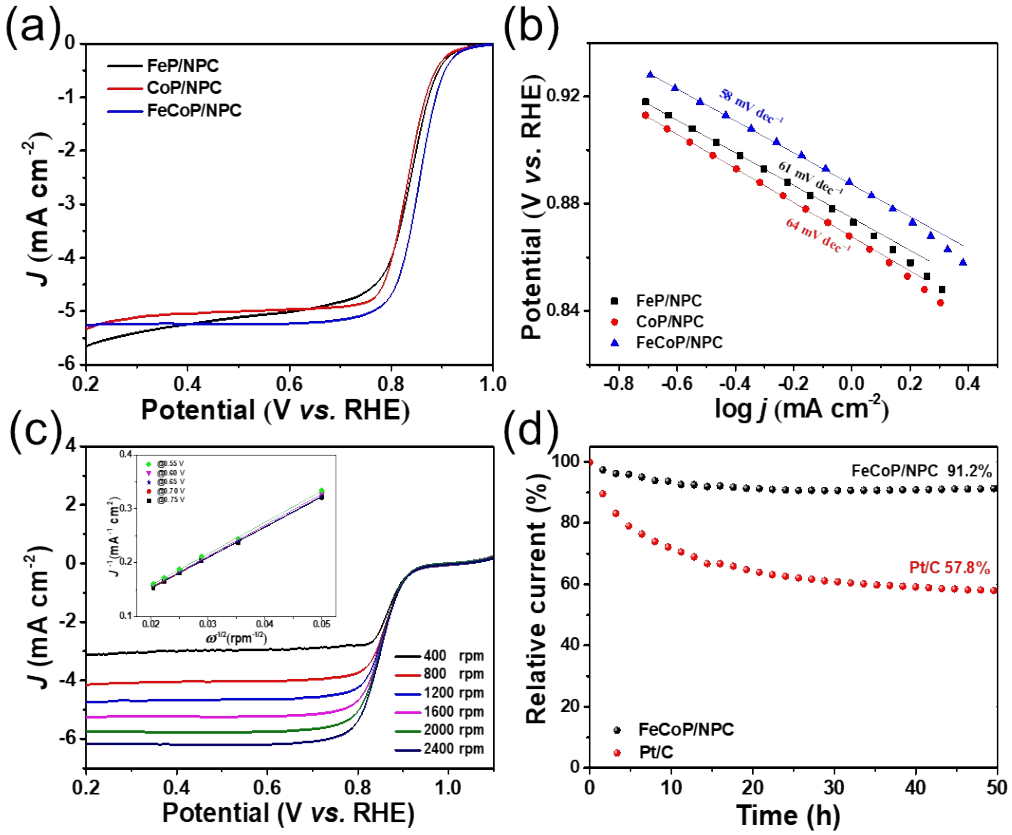

Figure S14. (a) ORR polarization curves of FeP/NPC, CoP/NPC and FeCoP/NPC electrocatalysts in O_2-saturated 0.1 M KOH solution at 1600 rpm. (b) Tafel slopes of FeP/NPC, CoP/NPC and FeCoP/NPC electrocatalysts. (c) LSV curves of FeCoP/NPC electrocatalyst at different rotation speed (inset: the corresponding K-L plots of FeCoP/NPC electrocatalyst at different potentials). (d) Chronoamperometric measurement (*i*-*t*) of FeCoP/NPC and Pt/C at 0.7 V.

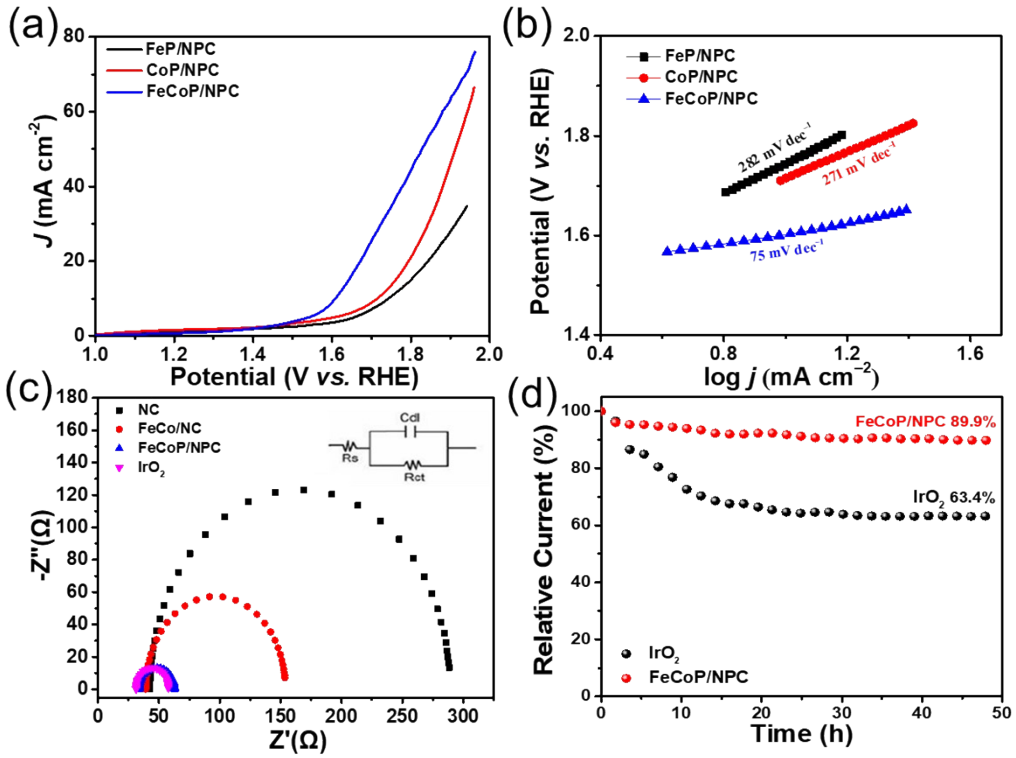

Figure S15. (a) OER polarization curves of FeP/NPC, CoP/NPC and FeCoP/NPC electrocatalysts in O_2-saturated 0.1 M KOH solution at 1600 rpm, (b) Tafel slopes of FeP/NPC, CoP/NPC and FeCoP/NPC electrocatalysts, (c) Impedance diagrams of NC, FeCo/NC, FeCoP/NPC and IrO_2, (d) Relative current versus time curves at 1.6 V of FeCoP/NPC and IrO_2.

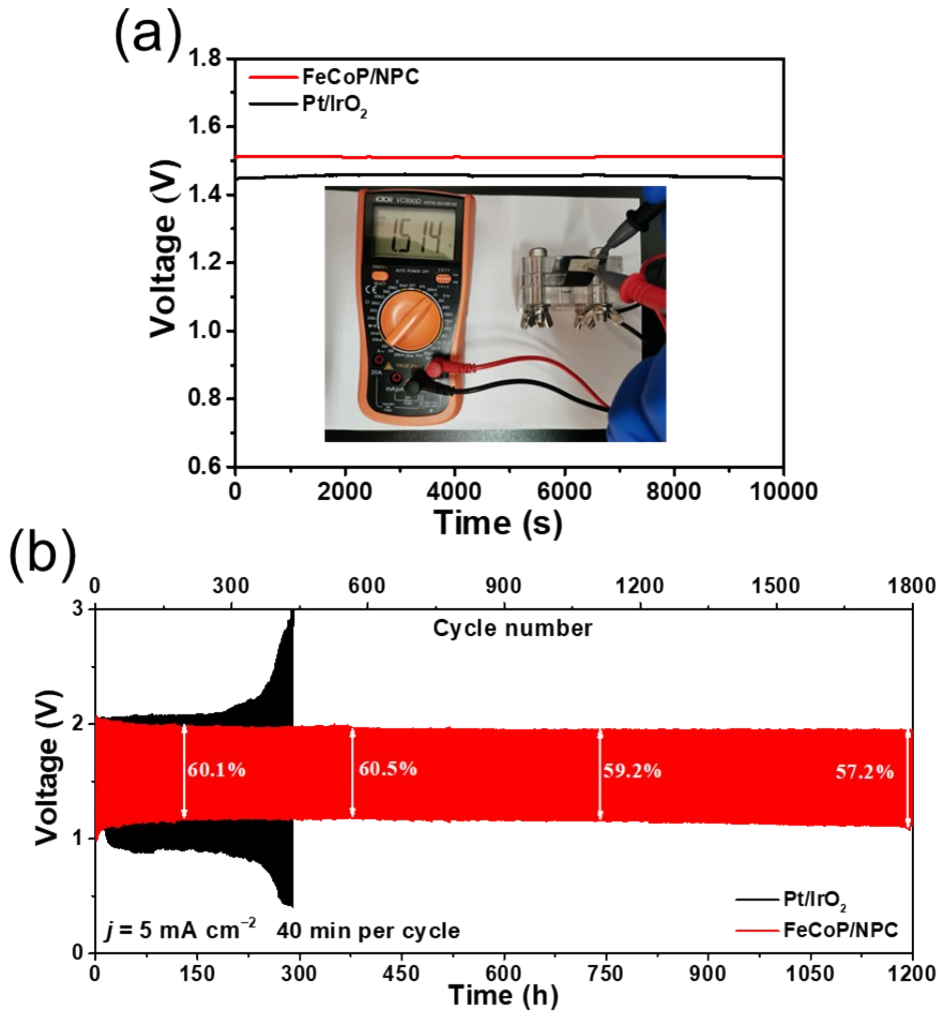

Figure S16. (a) Open-circuit voltage (OCV) plots (inset: photograph of FeCoP/NPC-based liquid Zn-air battery), (b) Galvanostatic discharging-charging cycle profiles of Pt/IrO_2 and FeCoP/NPC -based Zn-air battery at 5 mA cm^{-2} with a cycling interval of 40 min.

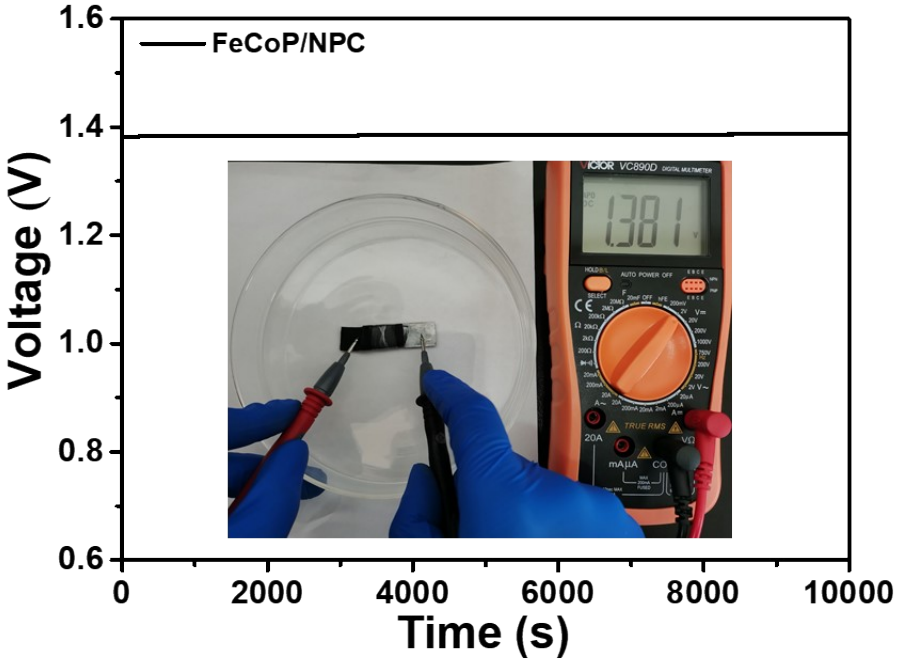

Figure S17. Open-circuit voltage (OCV) plots (inset: photograph of FeCoP/NPC-based solid Zn-air battery).

Table S1. Scrutinizing the ORR and OER performance of the as-synthesized electrocatalysts under various pyrolysis temperatures and compositions.

Catalysts	ORR	OER	ΔE
	$E_{1/2}$ (V *vs*. RHE)	$E_{j=10}$ (V *vs*. RHE)	
FeCoP/NPC-800	0.818	1.67	0.852
FeCoP/NPC-1000	0.803	1.63	0.905
FeCoP/NPC-1h	0.843	1.65	0.807
FeCoP/NPC-3h	0.738	1.64	0.902
FeCoP/NPC-1:10	0.793	1.61	0.817
FeCoP/NPC-1:14	0.818	1.66	0.842
FeCoP/NPC-1:3	0.833	1.65	0.817
FeCoP/NPC-1:1.5	0.818	1.67	0.852
FeCoP/NPC	0.855	1.61	0.755

Table S2. The specific surface areas (S_{BET}) and total pore volumes (V_t) of the as-synthesized electrocatalysts.

Electrocatalysts	S_{BET} (m^2 g^{-1})			V (cm^3 g^{-1})		
	Total	Micro	External	Total	Micro	External
FeCoP/NPC	**619.2**	**428.6**	**190.6**	**0.58**	**0.22**	**0.36**
NC	711.5	665.7	45.8	0.49	0.34	0.15
FeCo/NC	471.1	385.7	85.4	0.57	0.20	0.37
FeP/NPC	561.7	446.0	115.7	0.51	0.23	0.28
CoP/NPC	610.3	475.5	134.8	0.79	0.24	0.55

Table S3. ORR and OER activities of the as-synthesized electrocatalysts.

Electrocatalysts	ORR			OER		ΔE
	E_o (V *vs*. RHE)	$E_{1/2}$ (V *vs*. RHE)	$J_{@0.4}$ (mA cm^{-2})	$E_{j=10}$ (V *vs*. RHE)	$J_{@1.6}$ (mA cm^{-2})	
NC	0.963	0.853	5.11	1.94	2.05	1.087
FeCo/NC	0.930	0.835	5.08	1.75	2.80	0.915
FeP/NC	0.938	0.835	5.24	1.74	3.62	0.905
CoP/NC	0.938	0.833	5.04	1.71	4.89	0.877
FeCoP/NPC	**0.948**	**0.855**	**5.23**	**1.61**	**9.22**	**0.755**
Pt/C	0.973	0.843	5.80	N/A	N/A	0.777
IrO_2	N/A	N/A	N/A	1.62	8.11	

Table S4. The performances of FeCoP/NPC electrocatalysts for ORR/OER with those of phosphide-incorporated electrocatalysts reported in the literature.

Catalysts	$E_{1/2}$	$E_{j=10}$	ΔE	Ref.
FeCoP/NPC	**0.855**	**1.61**	**0.755**	**This work**
FeP/Fe_2O_3@ NPCA	0.838	1.632	0.794	2
$FeCo/Co_2P$@NPCF	0.79	1.56	0.77	3
Cu-Co_2P@2D-NPC	0.835	1.57	0.735	4
Co_2P@Co-NPG	0.808	1.728	0.92	5
CoNiP/PNC	0.84	1.70	0.86	6
Co_2P@CNF	0.803	1.69	0.887	7
CoO/Co_xP	0.86	1.60	0.74	8
Co_2P@NCNTs	0.82	1.75	0.93	9
$CoC_x/(Co_{0.55}Fe_{1.945})_2P$@C	0.84	1.62	0.78	10
Fe_2P@CNSs	0.84	1.63	0.79	11
Co-NC@CoP-NC	0.78	1.56	0.78	12
CoP@mNSP-C	0.90	1.64	0.74	13
CoP-DC	0.81	1.57	0.76	14

Note: All ORR/OER tests were conducted in 0.1 M KOH aqueous solution.

Table S5. Comparison of the FeCoP/NPC-based ZAB with those of phosphide-incorporated electrocatalysts reported in the literature.

Catalysts	Power Density (mW cm^{-2})	Stability of Cycles/Time	Ref.
FeCoP/NPC	**136**	**2475/1650 h @ 2 mA cm^{-2} 1800/1200 h @ 5 mA cm^{-2} 1425/950 h @ 10 mA cm^{-2}**	**This work**
FeP/Fe_2O_3@NPCA	130	1200/200 h @ 1 mA cm^{-2} 1020/170 h @ 5 mA cm^{-2} 756/126 h @ 10 mA cm^{-2}	2
FeCo/Co_2P@NPCF	154	642/107 h @ 10 mA cm^{-2}	3
Cu-Co_2P@2D-NPC	236	480/160 h @ charge 2 mA cm^{-2} discharge 10 mA cm^{-2}	4
CoO/Co_xP	122.7	400/200 h @ 5 mA cm^{-2}	8
CoNiP/PNC	171	57 h @ 10 mA cm^{-2}	6
Co_2P@CNF	103.5	55 h @ 2 mA cm^{-2}	7
CuCoP-NC-700	116.5	80/80 h @ 10 mA cm^{-2}	15
Co_2P/NPG	103.5	100/50 h @ 2 mA cm^{-2}	16
CoP/NP-HPC	186	240/80 h @ 2 mA cm^{-2}	17

References

[1] Jin T, Yin H, Easton C D, *European Polymer Journal*, 2019, **117**, 148-158.

[2] Wu K, Zhang L, Yuan Y, *Advanced Materials*, 2020, **32**, 2002292.

[3] Shi Q, Liu Q, Ma Y, *Advanced Energy Materials*, 2020, **10**, 1903854.

[4] Diao L, Yang T, Chen B, *Journal of Materials Chemistry A*, 2019, **7**, 21232-21243.

[5] Jiang H, Li C, Shen H, *Electrochimica Acta*, 2017, **231**, 344-353.

[6] Sun W, Xu Y, Yin P, *Applied Surface Science*, 2021, **554**, 149670.

[7] Gao J, Wang J, Zhou L, *ACS applied materials & interfaces*, 2019, **11**, 10364-10372.

[8] Niu Y, Xiao M, Zhu J, *Journal of Materials Chemistry A*, 2020, **8**, 9177-9184.

[9] Peng X, Liu Y, Hu S, *Journal of Alloys and Compounds*, 2021, **889**, 161628.

[10] Wu Y, Xiao Z, Jin Z, *Journal of Colloid and Interface Science*, 2021, **590**, 321-329.

[11] Fan H, Liu H, Hu X, *Journal of Materials Chemistry A,* 2019, **7**, 11321-11330.

[12] Li X, Jiang Q, Dou S, *Journal of Materials Chemistry A*, 2016, **4**, 15836-15840.

[13] Ahn S H, Manthiram A, *Small*, 2017, **13**, 1702068.

[14] Lin Y, Yang L, Zhang Y, *Advanced Energy Materials*, 2018, **8**, 1703623.

[15] Zhang H, Yang Z, Wang X, *Nanoscale*, 2019, **11**, 17384-17395.

[16] Shao Q, Li Y, Cui X, *ACS Sustainable Chemistry & Engineering*, 2020, **8**, 6422-6432.

[17] Wang Y, Wu M, Li J, *Journal of Materials Chemistry A*, 2020, **8**, 19043-19049.